Oxasmaragdyrin–Ferrocene and Oxacorrole–Ferrocene Conjugates: Synthesis, Structure, and Nonlinear Optical Properties

Sundararaman Venkatraman,[a] Rajeev Kumar,[a] Jeyaraman Sankar,[a] Tavarekere K. Chandrashekar,*[a] Kaladevi Sendhil,[b] C. Vijayan,[b] Alexandra Kelling,[c] and Mathias O. Senge[c]

Abstract: Ferrocenyl macrocyclic conjugates involving 22π oxasmaragdyrins and 18π oxacorroles have been synthesized and characterized. The direct covalent linkage of the ferrocenyl moiety to the *meso* position of the macrocycle is achieved by simple oxidative coupling of appropriate precursors with trifluoroacetic acid as catalyst. The electronic coupling between the ferrocenyl moiety and the macrocyclic π system is apparent from: a) the red shifts (293–718 cm^{-1}) of the Soret and Q-bands in the electronic absorption spectra of ferrocenyl conjugates; b) the shift of oxidation potentials (50–130 mV) of both the ferrocene and the corrole rings to the positive potentials; and c) considerable shortening of the C–C bond which connects the ferrocene and the *meso*-carbon atom of the macrocycle. The single-crystal X-ray structure of oxasmaragdyrin–ferrocene conjugate **9** reveals the planarity of the 22π skeleton with very small deviations of the *meso*-carbon atoms. The *meso*-ferrocenyl substituent has a small dihedral angle of 38°, making way for mixing of the molecular orbitals of the ferrocene and the macrocycle. However, the other two *meso* substituents are almost perpendicular to the mean plane, defined by the three *meso* carbon atoms. Classical C–H···O and nonclassical C–H···π interactions lead to a two-dimensional supramolecular network. Ferrocene–smaragdyrin conjugate **9** bonds to a chloride ion in the protonated form and a rhodium(I) ion in the free base form. Nonlinear optical measurements reveal a larger nonlinear refractive index (-5.83×10^{-8} cm^2W^{-1}) and figure of merit (2.28×10^{-8} cm^3W^{-1}) for the rhodium smaragdyrin–ferrocene conjugate **19** than for the others, suggesting its possible application in optical devices.

Keywords: conjugation · ferrocenyl conjugates · iron · nonlinear optics · porphyrinoids · supramolecular chemistry

Introduction

Research on the development of molecule-based electronic devices has gained momentum in recent years.[1] Discrete molecular conjugates are created by a covalent linkage of either a redox-active or a photoactive moiety to macrocycles having strong π-electron conjugation. Such conjugates are expected to show strong electronic interactions between the molecular components.[2] Specifically, the ferrocenyl groups have been used as redox-active groups with many macrocycles containing conjugated π electrons, for example with porphyrins to synthesize porphyrin–ferrocene conjugates.[3] The linkage between the porphyrin macrocycle and the ferrocenyl moiety plays an important role in inducing electronic interactions. There are many reports of one or more ferrocenyl moieties being linked to a porphyrin macrocycle through various spacer groups.[4] In such molecules the strength of electronic interaction depends on the nature of the spacer group, its length and its orientation. In most cases the spacer group has been observed to hinder the electronic contact, leading to weak communication between the molecular components. Therefore, for effective electronic communication, direct covalent linkage of the ferrocenyl groups with the porphyrin π system is a necessary requirement.

There are a few reports in the literature[5] of ferrocenyl groups being covalently linked directly to a porphyrin π system, without any spacer. Hendrickson and Wollmann[6] were the first to synthesize a porphyrin–ferrocene conjugate by refluxing pyrrole and ferrocene carboxaldehyde in propionic acid. However, the formation of atropisomers hin-

[a] S. Venkatraman, R. Kumar, J. Sankar, Prof. Dr. T. K. Chandrashekar
Department of Chemistry, Indian Institute of Technology
Kanpur 208016 (India)
Fax: (+91) 512-2597282/2597436/2590007
E-mail: tkc@iitk.ac.in

[b] K. Sendhil, Prof. Dr. C. Vijayan
Photonics Laboratory, Department of Physics
Indian Institute of Technology—Madras, Chennai 600036 (India)

[c] A. Kelling, Prof. Dr. M. O. Senge
Institut für Chemie, Universität Potsdam
Karl-Liebknecht-Strasse 24–25, 14476 Golm (Germany)

Supporting information for this article is available on the WWW under http://www.chemeurj.org/ or from the author.

 DOI: 10.1002/chem.200305558

dered the isolation of pure components. Later, Burrell, Officer and co-workers[5c] reported the synthesis and electrochemical properties of bis(ferrocenyl) porphyrin, in which two ferrocene groups, which are *trans* to each other, are linked to the porphyrin π system at the *meso* positions. This system shows strong electronic coupling between the porphyrin ring and the ferrocenyl groups. Kim and co-workers[5d] successfully synthesized mono-*meso*-substituted ferrocenyl porphyrin; they observed the presence of a π interaction between the porphyrin and ferrocene through ^{1}H NMR and electrochemical studies. Recently we were successful in synthesizing *meso*-ferrocenyl porphyrins containing one, two, three, and four ferrocenyl groups covalently linked to porphyrin *meso*-carbon atoms.[7] Electronic absorption and electrochemical studies on these systems suggest the presence of strong electronic communication between the ferrocenyl moiety and the porphyrin π system.

To the best of our knowledge, there are no reports in the literature on covalent linkage of ferrocenyl groups with either expanded or contracted porphyrins. Syntheses of expanded and contracted porphyrin–ferrocene conjugates are important in furthering the understanding of electronic communications between the macrocyclic π system and ferrocene. Herein we report such syntheses, as well as the characterization and spectroscopic, electrochemical, and nonlinear optical properties of expanded and contracted porphyrin–ferrocene conjugates. Specifically, we have chosen 22π oxasmaragdyrin **1** and 18π oxacorrole **2** as examples of expanded and contracted porphyrins, respectively, onto which to link covalently a ferrocenyl group at the *meso*-carbon bridge.

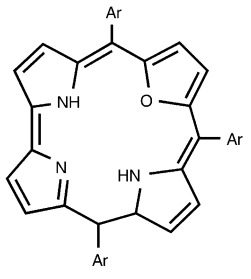

1

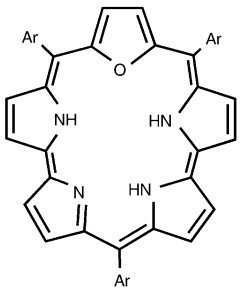

2

Electronic absorption studies on these systems reveal shifts in both the Soret and the Q-band absorption, to the order of 300–700 cm^{-1} relative to macrocycles without a ferrocenyl moiety, suggesting the presence of electronic communication. Single-crystal X-ray studies of the ferrocenyl–smaragdyrin conjugate **9** (see Figure 6) suggest almost perpendicular orientation of the ferrocenyl groups with respect to the smaragdyrin mean plane defined by the three *meso*-carbon atoms. Nonlinear optical properties of ferrocene–corrole and ferrocene–smaragdyrin conjugates studied by the *Z*-scan technique reveal a larger n_2 and figure of merit (FOM) value for rhodium smaragdyrin **19** (see Scheme 2), suggesting its possible application in optical devices. The electrochemical studies reveal a more positive oxidation potential for ferrocene in the conjugates than for free ferrocene.

Results and Discussion

Syntheses: The earlier synthesis of porphyrin–ferrocene conjugates in the literature is based on the classical condensation reaction of ferrocene carboxaldehyde with either pyrrole or dipyrromethane, followed by oxidation with chloranil. The formation of atropisomers by this method leads to separation problems,[6] to avoid which we have used a strategy by which the ferrocenyl moiety is covalently linked to one of the precursors and then the ferrocenyl precursor is used for the further condensation/coupling reactions. This will fix the orientation of the ferrocene group so that in the final product the possibility of formation of different atropisomers can be avoided. Specifically, we have synthesized ferrocenyl dipyrromethane by reaction of pyrrole and ferrocene carboxaldehyde using 0.01 equivalents of trifluoroacetic acid (TFA) as catalyst. This ferrocenyl dipyrromethane **3** was found to be stable, and thus amenable to complete spectral and X-ray crystallographic characterization. The structure of **3** (Figure 1) clearly reveals the orientation of the ferrocene group with respect to the dipyrromethane unit. There are no significant changes in the bond lengths of the ferrocene groups upon linkage to the dipyrromethane unit. The length of the C–C bond which connects the ferrocene group to the *meso*-carbon atom of dipyrromethane, C110–C19, is 1.56 Å. The torsion angles N11-C11-C19-C110 and N12-C15-C19-C110 are −64.4° and 176.6°, respectively.

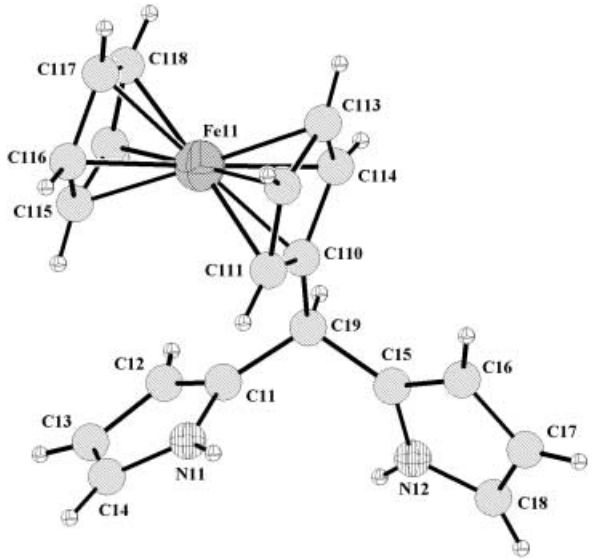

Figure 1. Single-crystal X-ray structure of **3**.

After we had obtained the required ferrocenyl dipyrromethane **3**, the standard acid-catalyzed "[3+2]" oxidative coupling methodology, which we had used earlier,[8] was followed to synthesize the ferrocenyl oxasmaragdyrins, in which two direct pyrrole–pyrrole bonds can be generated in

a single step. Thus, a coupling reaction between **3** and various *para*-substituted 5,10-diphenyl-16-oxatripyrranes **4–8** with 0.1 equivalents of TFA gave *meso*-ferrocenyl oxasmaragdyrins **9–13** as major products in ≈20% yield and the ring-contracted corroles **14–18** as a minor product (Scheme 1). The formation of corrole is attributable to the susceptibility to acid-catalyzed rearrangements of the dipyrromethane, which is known to undergo fragmentation; the fragmented products recombine to give corrole.[9]

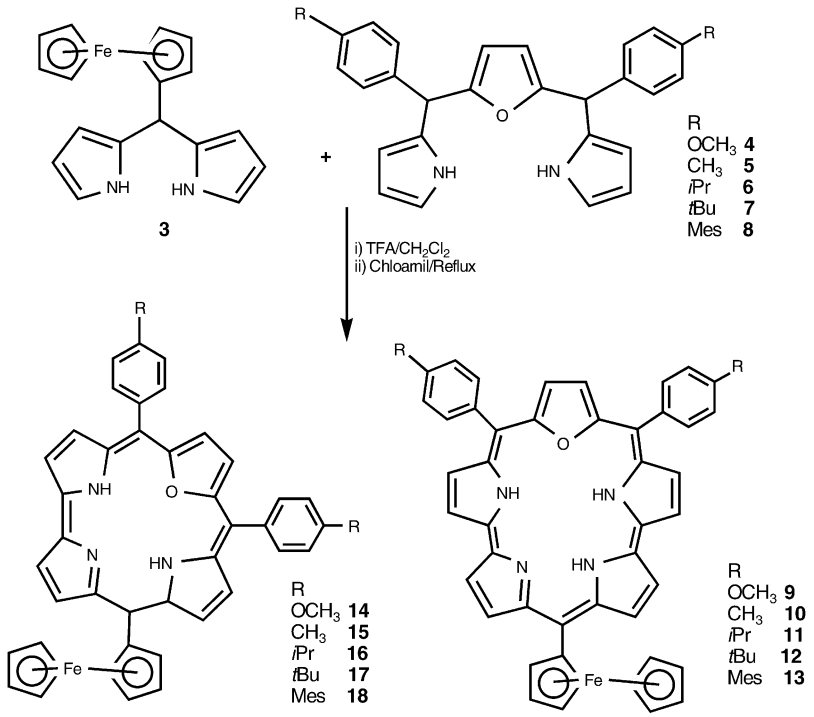

Scheme 1. Synthesis of *meso*-ferrocenyl oxacorroles and oxasmaragdyrins.

Both corroles and smaragdyrins were found to be stable as free bases in the solid and solution phases. The rhodium complex **19** was synthesized by the reaction of a solution of free base **9** in dichloromethane with di-μ-chlorobis[dicarbonylrhodium(I)] in the presence of sodium acetate. Monohydrochloride salt **20** was obtained by reaction of a solution of free base **9** in dichloromethane with HCl solution (10%). This also was quite stable (Scheme 2).

Spectral characterization: The FAB-mass spectra display molecular ion peaks at *m*/*z* 761 (100%) for **9** and 695 (80%) for **14**, confirming the proposed composition. The corresponding rhodium complex **19** exhibits peaks at *m*/*z* 918 (70%; see Supporting Information). The chloride complex of ferrocenyl smaragdyrin **20** shows a molecular ion peak at *m*/*z* 761 (100%), corresponding to loss of chloride ion under the FAB-mass conditions. Furthermore the presence of carbonyl groups in the rhodium complex was confirmed by IR spectroscopy, which displays peaks at 2072 and 2007 cm^{-1} for **19**. These frequencies compare well with those for rhodium–carbonyl complexes reported.[10]

^{1}H NMR spectroscopy: The ^{1}H NMR spectra of ferrocenyl oxasmaragdyrins **9–13** were well resolved in free base form and all the assignments were based on the correlations observed in the 2D COSY spectrum. For example, assignments for the well-resolved peaks in the ^{1}H NMR spectrum of **13** are marked in Figure 2: the bipyrrole protons (b, b′; c, c′; d, d′; e, e′) resonate as four well-resolved doublets in the δ = 8–10 ppm region. The outer bipyrrole protons (b′, e′; c′, d′) are closer to the ring current of ferrocene and the *meso*-phenyl groups than the other set of bi-

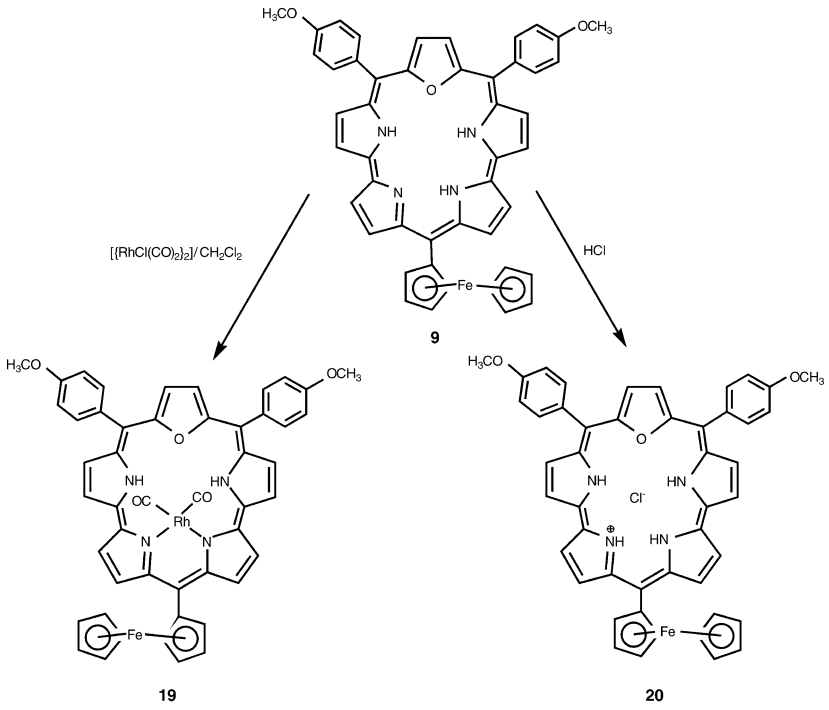

Scheme 2. Synthesis of rhodium and chloride complexes of *meso*-ferrocenyl oxasmaragdyrin.

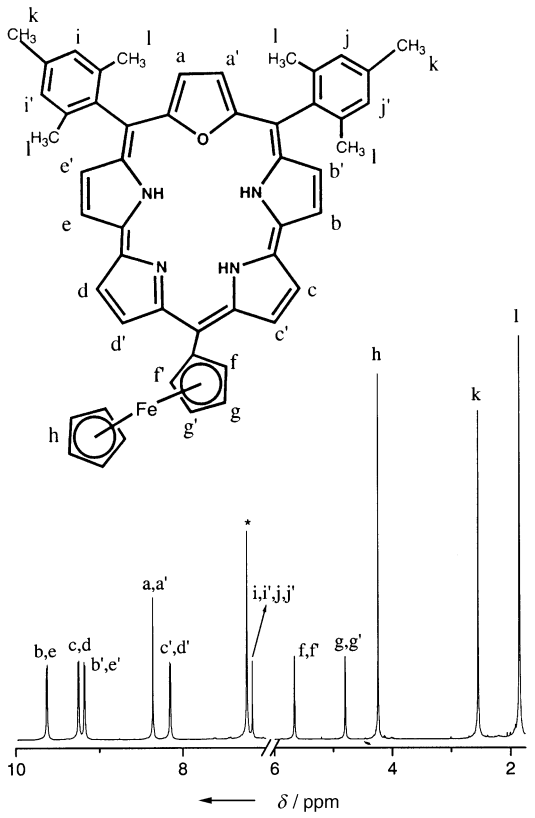

Figure 2. ^{1}H NMR spectrum of **13** at room temperature in $CDCl_3$. The assignments are marked on the basis of correlations observed in ^{1}H–^{1}H COSY.

pyrrolic protons (b, e; c, d) and hence they are slightly shielded. The β-CH protons of the furan ring (a, a′) appear as a sharp singlet at $\delta = 8.36$ ppm. There are three sets of protons for the *meso*-ferrocenyl group. The protons present next to the carbon atom at the *meso* position (f, f′) resonate at $\delta = 5.66$ ppm and the other two protons (g, g′) resonate at $\delta = 4.79$ ppm; the other cyclopentadienyl ring protons resonate as a singlet at $\delta = 4.24$ ppm. The equivalence of the bipyrrole protons (b′, e′; b, e; c, d; c′, d′) in the ^{1}H NMR spectrum suggest that the three −NH protons exchange sites between the four bipyrrole nitrogen centers, indicating that the molecule adopts a symmetric conformation in solution with respect to the mirror plane passing through the methine bridge connecting ferrocene and the furan oxygen atom. This is possible only if there is a rapid tautomerism between the inner −NH protons. To arrest this tautomerism the ^{1}H NMR spectrum was recorded at lower temperatures. Up to 233 K no peak was observed in the shielded region, suggesting the presence of rapid tautomerism even at low temperatures. However, at 233 K a sharp peak was observed at $\delta = -2.33$ ppm with an integration corresponding to two protons (see the Supporting Information). This suggests that at 233 K, from among three −NH protons, the two in one bipyrrole ring system are localized and the third one, in the other bipyrrole ring, is still exchanging sites with the two pyrrole nitrogen atoms of the bipyrrole ring system. Introduction of Rh^I to ferrocenyl smaragdyrin conjugate **9** gives the corresponding rhodium complex **19**, in which rhodium is bound in an η^2 fashion to only two of the four core nitrogen atoms and the other two coordination sites are occupied by the ancillary carbonyl ligands. In this bonding mode, the two inner −NH protons on the bipyrrole unit are not exchangeable. Thus, as expected in **19**, these inner −NH signals are seen at $\delta = -1.43$ ppm, not only confirming the rhodium coordination but also revealing the arrest of NH tautomerism upon metal coordination. The bipyrrole protons (d, d′; c, c′) experience a small upfield shift (0.27–0.31), while the bipyrrole protons (b, b′; e, e′) are not affected by the metal coordination. This observation further confirms our earlier findings that the Rh^I prefers to bond to the bipyrrolic rings with one amino and one imino nitrogen.[10a]

The ^{1}H NMR spectra of ferrocenyl oxacorroles **14**–**18** are not as simple as those of ferrocenyl oxasmaragdyrins. β-CH protons of each pyrrole and furan resonate as distinct signals, which reflect the lower symmetry of the molecule. The furan protons (a, a′), two bipyrrolic protons (b, b′; d, d′), and pyrrole protons (c, c′) each resonate as doublets in the aromatic region ($\delta = 8.2$–9.6 ppm) for **14**. Characteristic sets of cross peaks resulting from the coupling of furan (a, a′), pyrrole (c, c′), and bipyrrole (b, b′; d, d′) have been established from the assignments based on correlations in 2D COSY (Figure 3). The *ortho*- and *meta*-hydrogen atoms present in the *meso*-phenyl groups appear as two sets of resonances, and in turn show the correlations of i, i′; k, k′ with h, h′ and j, j′ protons as indicated.

In the shielded region a sharp peak at $\delta = -1.42$ ppm corresponding to an integration of two protons was observed at 298 K for **14**. This observation suggests the equivalence of both −NH protons. Upon protonation with TFA, at 273 K (Figure 4) there are three distinct signals in the region $\delta = -1.5$ to -3.5 ppm corresponding to three −NH protons. This is expected, because it is well known that upon protonation due to the steric crowding, the corrole core becomes ruffled to avoid steric repulsion between the protons inside the core.[11] Furthermore, of the three signals, the peak at $\delta = -1.7$ ppm was found to be much sharper than the other two. This observation we attribute to the possible weak hydrogen bonding interaction of the −NH proton with the furan oxygen atom present in the same plane.[5d]

Electronic absorption spectra: Typical electronic absorption spectra observed for oxasmaragdyrin–ferrocene and oxacorrole–ferrocene conjugates **9** and **14** are shown in Figure 5. In both the cases a strong Soret-type band in the region 400–500 nm and weak Q-bands in the region 500–800 nm confirm the porphyrinic nature. The UV/Vis data (Table 1)demonstrate that:

a) The ε values of the ferrocenyl conjugates are more than 50% lower than those of **1** or **2**, suggesting a strong electronic interaction between the ferrocene and the macrocyclic π system. This drastic decrease in the ε value is the result of extensive mixing of both the ferrocene molecular orbitals and the molecular orbitals of either the smaragdyrin or the corrole ring. A similar observation was made by Burrell and co-workers[5c] for bis(ferrocenyl) porphyrin systems.

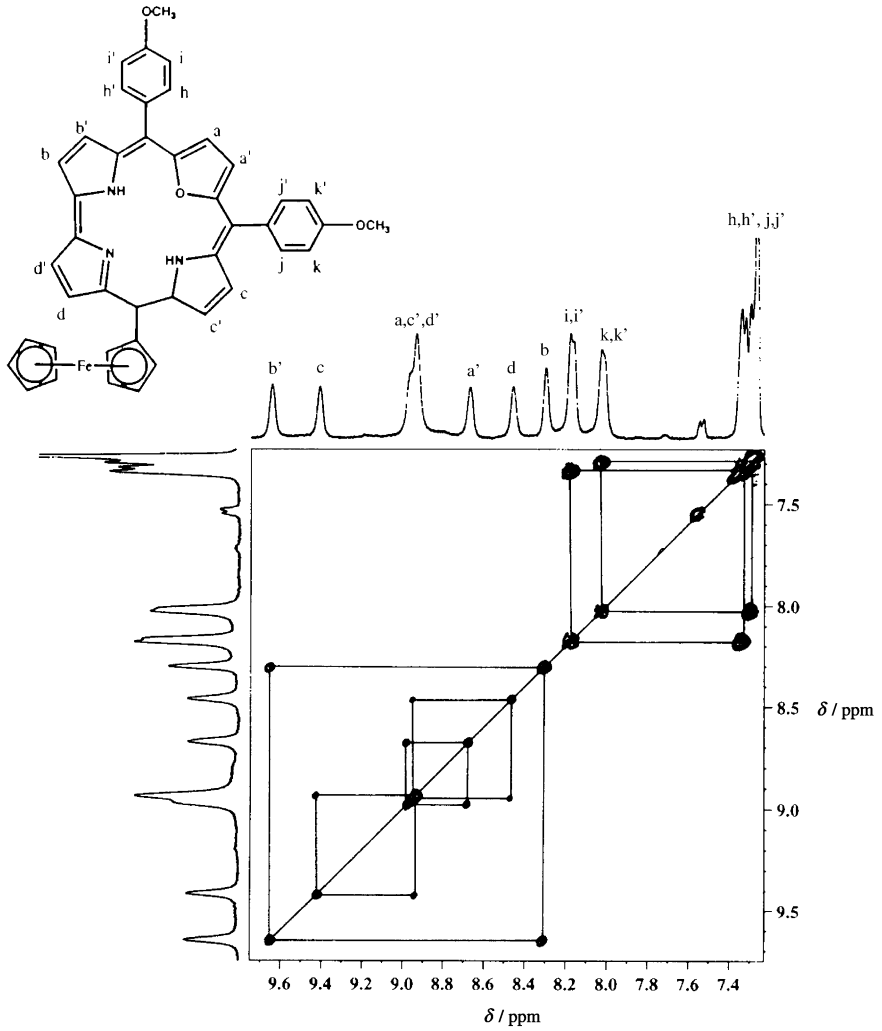

Figure 3. ^{1}H–^{1}H COSY spectrum of **14** in $CDCl_3$ at room temperature. The observed correlations are marked.

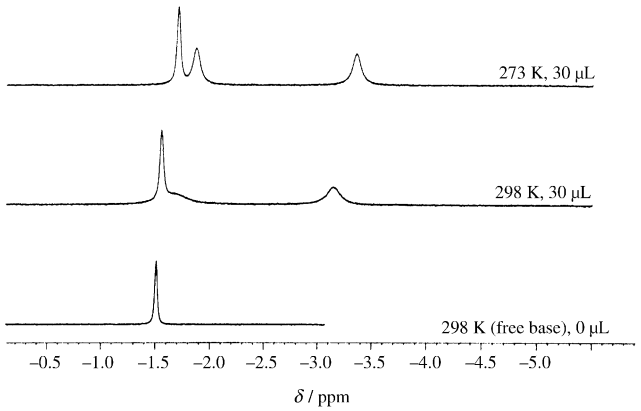

Figure 4. Chemical shift dependence of inner NH protons on temperature and concentration of TFA for **14**. The volume of TFA added and the temperature are indicated.

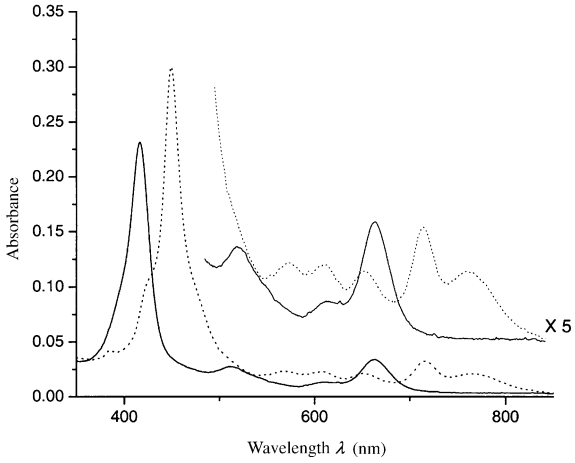

Figure 5. Electronic absorption spectra of **9** (-----) (1.65×10^{-6} M) and **14** (——) (2.52×10^{-6} M) in dichloromethane.

Soret band (293–302 cm^{-1}) and is similar to that observed for the *meso*-ferrocenyl porphyrins.[7]

c) Metalation of **9** with rhodium results in a considerable red shift in both Soret and Q-bands relative to the corresponding free base form.

Taken together these observations collectively give strong evidence for the presence of electronic interaction between the ferrocene moiety and the porphyrin π system in ferrocenyl conjugates.

Crystallographic characterization: The single-crystal X-ray structure of smaragdyrin–ferrocene conjugate **9** is shown in Figure 6. One molecule of methanol is trapped inside the cavity. The important crystallographic parameters are listed in Table 2. The side view of the structure indicates small deviations from planarity (Figure 6b). The deviations of the heterocyclic rings from the mean smaragdyrin plane (defined by the three *meso*-carbon atoms C1, C6, and C15 which form the plane) are: for the furan, 13.7°; for the pyrrole N1 ring 18.1°; for the pyrrole N2 ring, 8.52°; for the pyrrole N3 ring, 14.9°; for the pyrrole N4 ring, 21.42°. These deviations are similar to that observed for **2**, suggesting that there is not much structural de-

b) The ferrocene substitution results in a bathochromic shift of both the Soret and the Q-bands in the ferrocene conjugates relative to **1** or **2**. The magnitude of the Q-band shifts is higher (401–763 cm^{-1}) than those for the

Table 1. UV/Vis absorption data for ferrocene–corrole and ferrocene–smaragdyrin conjugates in the Soret and Q-band region in dichloromethane ($\approx 10^{-6}$ M).

Compound	λ_{max} [nm] ($\varepsilon \times 10^{-4}$ [$mol^{-1} dm^3 cm^{-1}$])				
	Soret	Q-bands			
2	443 (33.0)	552 (2.0)	591 (1.4)	633 (1.0)	696 (1.4)
9	449 (18.1) [302][a]	567 (1.4) [479][a]	607 (1.4) [446][a]	653 (1.3) [484][a]	716 (2.0) [401][a]
10	449 (14.9) [302][a]	570 (1.3) [573][a]	604 (1.2) [364][a]	651 (1.0) [438][a]	714 (1.5) [363][a]
11	449 (17.8) [302][a]	570 (1.5) [572][a]	603 (1.4) [337][a]	649 (1.3) [389][a]	714 (1.9) [363][a]
12	449 (14.8) [302][a]	567 (1.9) [480][a]	607 (1.7) [446][a]	649 (1.5) [389][a]	716 (2.6) [401][a]
13	449 (13.1) [302][a]	567 (0.9) [480][a]	606 (0.9) [420][a]	650 (0.8) [414][a]	715 (0.1) [382][a]
1	411 (27.0)	497 (1.6)	528 (1.6)	583 (0.7)	632 (0.4)
14	416 (9.2) [293][a]	–	511 (1.1) [630][a]	–	664 (1.4) [763][a]
15	417 (7.1) [351][a]	–	510 (0.7) [668][a]	–	662 (1.0) [718][a]
16	416 (8.8) [293][a]	–	512 (0.9) [592][a]	–	662 (1.2) [718][a]
17	416 (7.9) [293][a]	–	509 (1.0) [707][a]	–	662 (0.9) [718][a]
18	415 (7.7) [235][a]	–	508 (0.7) [746][a]	–	659 (1.0) [648][a]

[a] Shift [cm^{-1}] with respect to *meso* aryl analogues.

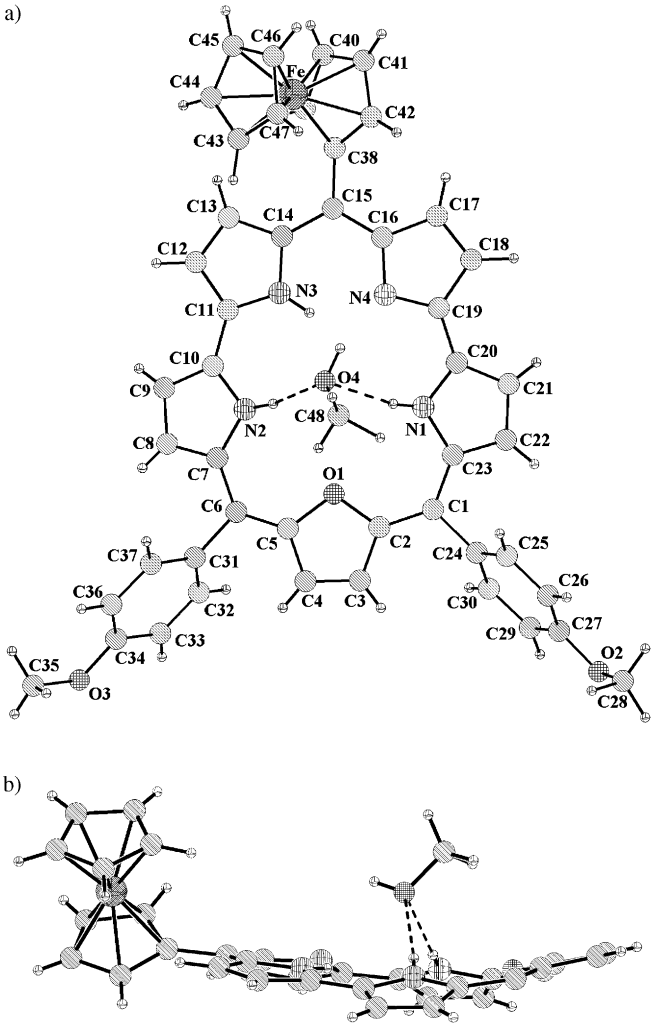

Figure 6. Single-crystal X-ray structure of **9** with one trapped methanol molecule: a) top view; b) side view (*meso*-phenyl rings are omitted for clarity).

viation upon ferrocene substitution.[8] The dihedral angle (38°) between the smaragdyrin plane and the cyclopentadienyl ring of ferrocene is much smaller than that reported for mono(*meso*-ferrocenyl) porphyrin by Kim and co-workers,[5d] due to the absence of any of the β-pyrrole substituents present in Kim's system. This small dihedral angle makes possible a weak π overlap between the cyclopentadienyl ring and the smaragdyrin skeleton. This possibility is further reflected in the bond distances observed. The C–C bond (C15–C38) connecting the ferrocenyl ring to the *meso*-carbon atom is 1.473 Å long. The corresponding bond length (C19–C110) in the ferrocenyl dipyrromethane **3** is 1.516 Å. Furthermore the C–C bond lengths of the remaining two *meso*-phenyl substituents (C1–C24; C6–C31) are 1.505 Å

Table 2. Crystallographic data for ferrocenyl dipyrromethane and ferrocene–smaragdyrin conjugate.

Crystallographic data	**3**	**9**
solvent for crystallization	CH_2Cl_2	CH_2Cl_2/MeOH
empirical formula	$C_{38}H_{36}Fe_2N_4$	$C_{48}H_{40}FeN_4O_4$
T [K]	293(2)	210
crystal system	monoclinic	triclinic
space group	$P2_1/n$	$P\bar{1}$
V [Å^3]	3097(2)	1872.9(4)
a [Å^3]	15.576(5)	9.9376(11)
b [Å^3]	7.774(5)	12.6375(14)
c [Å^3]	25.722(5)	15.927(2)
α [°]	90.000(5)	74.305(9)
β [°]	96.017(5)	76.565(9)
γ [°]	90.000(5)	86.639(9)
Z	4	2
ρ_{calcd} [$Mg\,m^{-3}$]	1.408	1.406
measured reflections	5651	35256
unique reflections	5449	6579
R(in)	0.0218	0.0502
F(000)	1360	828
limiting indices	$-18 \le h \le 18$, $0 \le k \le 9$, $-30 \le l \le 0$	$-11 \le h \le 11$, $-15 \le k \le 15$, $-18 \le l \le 18$
GoF (F^2)	0.989	0.901
final R indices [$I > 2\sigma(I)$]		
R_1	0.0356	0.0384
wR_2	0.1084	0.0896
R indices (all data)		
R_1	0.0457	0.0628
wR_2	0.1159	0.0954

and 1.50 Å, respectively. Thus, the significant reduction in the bond length of C15–C38 for **9** clearly suggests the presence of electronic coupling between the ferrocenyl moiety and the smaragdyrin π system. This C–C bond length, 1.473 Å, falls within the range of the distances observed for other ferrocene–porphyrin conjugate systems (1.47–1.49 Å), where strong π electronic communications are seen.[5c] The dihedral angles, 64.2° and 61.1°, of the two remaining *meso*-phenyl substituents with the mean smaragdyrin plane suggest that no effective π overlap exists between the macrocyclic π system with the phenyl rings and hence the C–C bond lengths remain unaltered. The aromatic nature of the 22π oxasmaragdyrin is further confirmed by the C_β–C_β bond lengths of the heterocyclic rings. For example, the C_β–C_β bond length in the furan ring is 1.347 Å, whereas the C_α–C_β bond length is 1.409 Å. This agrees well with data for expanded porphyrins reported in the literature.[12]

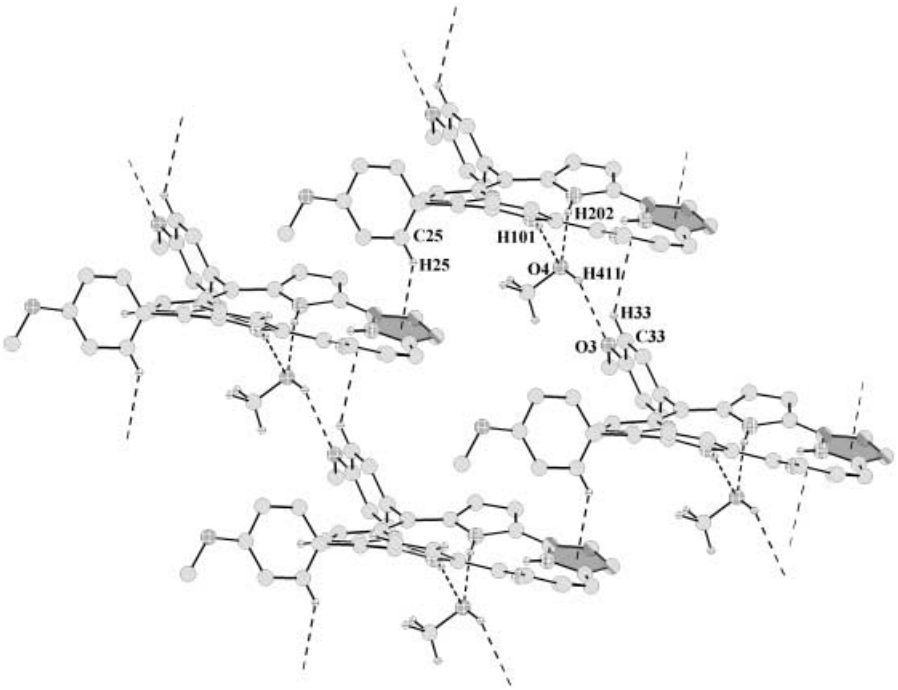

Figure 7. A view of the two-dimensional array formed by **9**. The secondary interactions are shown by broken lines. Non-interacting hydrogen atoms and ferrocenyl units are omitted for clarity; pyrrole rings involved in C–H···π interactions have been shaded.

Another important observation on the crystal structure of **9** is that one methanol solvent molecule is trapped inside the cavity of the macrocycle. The solvent methanol is held by two hydrogen-bonding interactions between the methanol oxygen and the hydrogen atoms attached to the pyrrole N2 and N1 rings (O4···H202, 2.149 Å, 162.2°; O4···H101, 2.213 Å, 160.4°). Furthermore, the hydroxyl hydrogen atom of the trapped solvent (methanol) is involved in the hydrogen-bonding interaction with the oxygen atom of the *para*-methoxyphenyl substituent of the neighbouring smaragdyrin skeleton (O3···H411, 2.370 Å, 141.9°). In addition, there is another strong hydrogen-bonding interaction involving the C–H of the *meso*-phenyl substituents and the pyrrole π cloud of dipyrromethane containing the ferrocene unit, leading to C–H···π interactions. This process extends further in other directions, leading to a two-dimensional layer structure (Figure 7). The metric parameters for C–H···π interactions are: C25–H25···π centroid, 2.741 Å, 135.1°; C33–H33···π centroid, 2.642 Å, 141.8°.

Electrochemical studies: The redox behavior of various ferrocene–oxacorrole conjugates was monitored by cyclic voltammetric studies using 0.1 M $TBAPF_6$ (tetra-*n*-butylammonium hexafluorophosphate) as the supporting electrolyte in CH_2Cl_2, in the potential range −1.8–1.8 V versus Ag/AgCl. A typical cyclic voltammogram overlaid with a differential pulse voltammogram of **14**, scanned towards the positive potential, is shown in Figure 8. Table 3 shows the half-wave reduction potentials along with free ferrocene and oxacorrole **1**. Δ_{redox}, calculated from the difference between the first oxidation potential and the first reduction potential, indicates significant decreases relative to **1** (2.18 V). This observation suggests a decrease in the HOMO–LUMO gap in ferrocenyl corrole conjugates relative to **1**, which is consistent with the red shifts of the Soret and the Q-bands in the electronic absorption spectrum. In general ferrocene–corrole conjugates show three quasi-reversible oxidations (ΔE_p = 70–130 mV), of which one is based on the ferrocene and the other two on the corrole rings. That the ferrocenyl oxidation is 50 mV more positive than that of free ferrocene indicates the effect of ferrocenyl substitution in ferrocenyl conjugates. This observation contrasts with those for mono- and bis(*meso*-ferro-

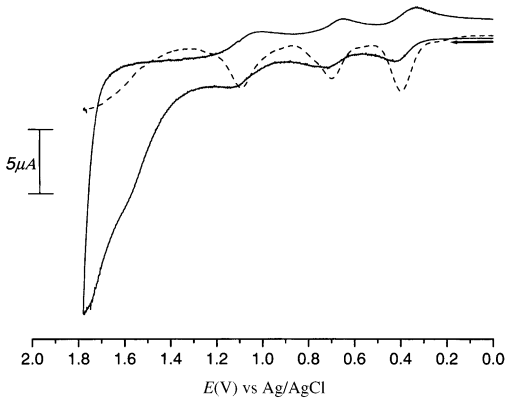

Figure 8. Cyclic voltammograms (——) and differential pulse voltammograms (-----) of **14** in dichloromethane containing 0.1 M $TBAPF_6$ recorded at 100 mV s^{-1} scan speed.

Table 3. Electrochemical data for ferrocene–corrole conjugates, free ferrocene and *meso* aryl oxacorrole.

Compound	Corrole ring $E_{1/2}^{red}(1)$ [V]	Corrole ring $E_{1/2}^{red}(2)$ [V]	$E_{1/2}^{ox}(1)$ [V]	Ferrocenyl ring $E_{1/2}^{ox}(2)$ [V]	Δ_{redox}[a]	$E_{1/2}^{ox}$ [V]
Ferrocene	–	–	–	–	–	0.37
1	−1.46	–	0.72	–	2.18	–
16	−1.08	−1.41	0.81	1.09	1.89	0.42
17	−1.08	−1.41	0.79	1.09	1.87	0.42
18	−1.21	−1.49	0.85	1.19	2.06	0.42
14	−1.32	−1.58	0.78	0.99	2.10	0.42

[a] Calculated from difference between $E_{1/2}^{ox}(1)$ and $E_{1/2}^{red}(1)$.

cenyl) porphyrins,[5c,d] where the electron-rich β pyrrole substituents make the porphyrin ring electron-releasing and thus oxidation becomes easier. In the present case, the absence of β-substituents probably makes the corrole moiety electron-deficient and hence the potentials are shifted to the more positive side as expected. On the other hand, the corrole-based oxidations and reductions show the opposite trend. Corrole ring oxidations show a positive shift (60–130 mV), while the corrole ring reduction potentials are shifted in the negative direction (140–380 mV) relative to **1** upon ferrocenyl substitution. The shift of oxidation potentials to the more positive side is due to a combination of the electronic coupling between the corrole π system and the ferrocene moiety, with the nonplanarity of the corrole ring.[13] The less negative ring reduction potentials are consistent with the electron deficiency of the corrole ring in the ferrocenyl conjugates relative to oxacorrole **1**.

Nonlinear optical studies: Figure 9 shows the typical refractive *Z*-scan trace for **19**. The open squares indicate the experimentally obtained data and the broken line was generated theoretically using the *Z*-scan theory[14] for a nonlinear phase shift of less than π. The values of the nonlinear refractive index n_2 calculated using the Sheik-Bahae formalism[14] and the figure of merit (FOM) for the four samples are tabulated in Table 4. All the samples show a *Z*-scan trace indicative of a defocusing material with a negative nonlinear refractive index. There was no contribution to the nonlinear absorption by the samples at this input power level, as can be deduced from the symmetry of the *Z*-scan traces; this was confirmed by an open *Z*-scan experiment which returned a negative result. Since all the compounds have negative n_2 values and the probing source is a continuous-wave laser, the origin of the nonlinearity is predominantly thermal. From the table, the n_2 value, which is a measure of the nonlinear response exhibited by the molecule, decreases on going from ferrocene–oxasmaragdyrin to ferrocene–oxacorrole conjugates. The higher value observed for smaragdyrin is attributed to a larger π electron conjugation (22π) for smaragdyrin relative to corrole (18π).

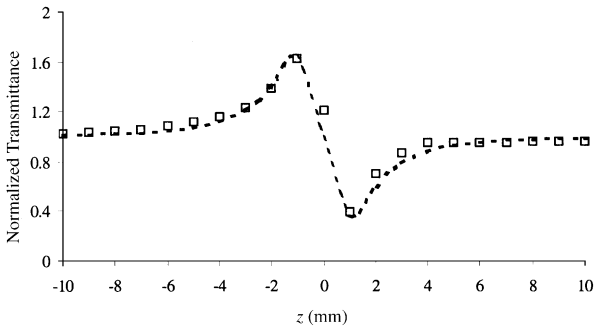

Figure 9. Closed *Z*-scan trace of **19** in dichloromethane ($\approx 10^{-4}$ M) under continuous-wave laser illumination. Open squares represent experimental data and the broken line is generated theoretically.

Table 4. Linear absorption coefficient, nonlinear refractive index and FOM data obtained from *Z*-scan technique.

Compound	α [cm^{-1}]	$n_2 \times 10^8$ [cm^{2}W^{-1}]	FOM $\times 10^8$ [cm^{3}W^{-1}]
19	2.56	−5.83	2.28
20	2.77	−4.61	1.66
9	2.64	−2.77	1.05
14	2.31	−0.43	0.19

A good material for optical devices should absorb least from the input source and exhibit as high a nonlinear response as possible. The FOM, defined as the ratio n_2/α, was calculated for all four compounds. The FOM values also show a decrease on going from smaragdyrin to corrole. Materials with larger FOM values are known to be more suitable for device applications, since they combine a larger nonlinearity with a low linear absorption coefficient; therefore the loss during operation of an optical device based on such compounds will be minimal. In the compounds studied here, the rhodium complex of smaragdyrin **19** stands out, with larger FOM values, than the others.

Conclusion

Successful synthesis of ferrocenyl conjugates with one expanded porphyrin and one contracted porphyrin is achieved by employing "[3+2]" acid-catalyzed oxidative coupling of appropriate precursors. The direct covalent linkage of the ferrocenyl moiety to the *meso*-carbon atom of the macrocycle leads to strong electronic communication between the ferrocenyl moiety and the macrocycle π system, as observed from spectroscopic and electrochemical measurements. The single-crystal X-ray structure of **9** confirms the proposed structure. The secondary interaction involving C−H···O and C−H···π in the crystal packing leads to a two-dimensional supramolecular network in the solid state. Preliminary nonlinear optical measurements reveal decent values of n_2 and FOM for the rhodium–smaragdyrin conjugate **19**, giving promise for its application in optical devices. Detailed studies in this direction are under way in our laboratory.

Experimental Section

Instrumentation: Electronic spectra were recorded on a Perkin-Elmer Lambda 20 UV/Vis spectrophotometer. Proton NMR spectra in $CDCl_3$ were obtained on a 400 MHz JEOL spectrometer, and FAB-MS spectra on a JEOL-SX-120/DA6000 spectrometer.

X-ray crystallographic studies: The crystals were immersed in hydrocarbon oil (Paraton N), and a single crystal was selected, mounted on a glass fibre and placed in the low-temperature N_2 stream.[15] Intensity data were collected at 210 K with a Stoe IPDS2 system utilizing $Mo_{K\alpha}$ radiation (λ = 0.71073 Å). The intensities were corrected for Lorentz and polarization effects. The structure was solved by direct methods using the SHELXTL PLUS program system[16a] and refined against $|F^2|$ with the program XL-97 using all the data.[16b] Non-hydrogen atoms were refined with anisotropic thermal parameters. Hydrogen atoms were located in difference maps and refined using a ridging model.

CCDC-219937 (for **3**) and CCDC-219938 (for **9**) contain the supplementary crystallographic data for this paper. These data can be obtained free of charge via www.ccdc.cam.ac.uk/conts/retrieving.html (or from the Cambridge Crystallographic Centre, 12 Union Road, Cambridge CB21EZ, UK; Fax: (+44) 1223-336-033; or deposit@ccdc.cam.ac.uk).

Nonlinear optical studies: Nonlinear optical studies were done for **9**, **14**, **19**, and **20** by the well-known *Z*-scan technique developed by Sheik-Bahae et al.[14] The nonlinear refractive index (n_2) was determined from a closed *Z*-scan experiment, in which the He–Ne laser (TEM_{00} output; power 20 mW) was focused to a spot of radius 7.5 μm by a lens of focal length 75 mm, and a photodetector fitted with an aperture of radius 0.6 mm was used to collect the output from the exit plane of the sample. The intensity at the focus of the lens was $\approx 1.6\times10^8$ W m^{-2}. It was ensured that the thickness of the sample was well within the Rayleigh limit of the Gaussian input beam. The sample was moved along the beam direction in the focal region in millimetre steps with the help of a micro-controlled stepper motor. The photodetector output was fed into a computer. All four samples were prepared at concentrations of $\approx 10^{-4}$ M in dichloromethane to ensure uniformity of measurement and ease of comparison. The solvent was found to have a negligible effect on the n_2 value at this power level and wavelength. The linear optical absorption coefficient of all the samples was maintained at $\approx$2–3 cm^{-1} to ensure the same level of absorption and nonresonant interaction.

Chemicals: All NMR solvents were used as received. Solvents such as dichloromethane, tetrahydrofuran and *n*-hexane were purified and distilled by standard procedures. $TBAPF_6$ from Fluka was used as the supporting electrolyte for cyclic volatammetric studies. 2,5-Bis(phenylhydroxymethyl)furan and 16-oxatripyrranes **4**–**8** were prepared according to the published procedure[17] and stored under an inert atmosphere at −10 °C.

Syntheses

***meso*-Ferrocenyl dipyrromethane (3)**: A mixture of pyrrole (6.48 mL, 93 mmol) and ferrocene carboxaldehyde (0.5 g, 2.3 mmol) was degassed by bubbling argon for 10 min. Trifluoroacetic acid (0.036 mL, 0.23 mmol) was added and the mixture was stirred for 30 min at room temperature. It was diluted with CH_2Cl_2 (100 mL), and then washed with 0.1 M NaOH, then with water. The organic layer was dried over anhydrous sodium sulfate. The solvent was removed under reduced pressure and the unreacted pyrrole was removed by vacuum distillation at room temperature. The resulting viscous, dark yellow liquid was purified by column chromatography (silica gel (100–200 mesh), ethyl acetate/petroleum ether (7:93)). After the initial tailing material, a pale yellow solid **3** was identified as *meso*-ferrocenyl dipyrromethane. Yield 47%; EI: *m*/*z* (%): 330 (95) $[M+1]^+$; ^{1}H NMR (400 MHz, $CDCl_3$, 25 °C): δ = 4.09 (s, 7H), 4.19 (s, 2H), 5.2 (s, 1H), 6.00 (m, 2H), 6.13 (m, 2H), 6.65 (s, 2H), 7.93 ppm (br s, 2H); elemental analysis: calcd (%) for $C_{19}H_{17}FeN_2$: C 69.32, H 5.21, N 8.51; found: C 69.66, H 6.01, N 8.76.

5,10-(*p*-Methoxydiphenyl)-19-ferrocenyl-25-oxasmaragdyrin (9) and 5,10-(*p*-methoxydiphenyl)-15-ferrocenyl-21-oxacorrole (14): The 16-oxatripyrrane **4** (0.642 g, 1.46 mmol) and ferrocenyl dipyrromethane (**3**, 0.485 g, 1.46 mmol) were dissolved in dry dichloromethane (600 mL) and stirred under a nitrogen atmosphere for 5 min. TFA (0.011 mL, 0.146 mmol) was added and the stirring continued for further 90 min. Chloranil (1.077 g, 4.38 mmol) was added and the reaction mixture was exposed to air and refluxed for a further 90 min. The solvent was evaporated in vacuo. The residue was purified by chromatography on a basic alumina column. The brown fraction, which eluted with petroleum ether/dichloromethane (10:90), was identified as mono-oxacorrole **14** (0.020 g, 3%), which decomposes above 280 °C. The second green band, eluted with dichloromethane/ethyl acetate (85:15), gave **9** (0.17 g, 20%), which decomposes above 300 °C.

9: FAB-MS: *m*/*z* (%): 761 (100%) $[M^+]$; ^{1}H NMR (400 MHz, $CDCl_3$, 25 °C, TMS): δ = 9.67 (d, *J* = 4.4 Hz, 2H), 9.30 (d, *J* = 4.4 Hz, 2H), 9.23 (d, *J* = 4.4 Hz, 2H), 8.58 (s, 2H), 8.28 (d, *J* = 4.4 Hz, 2H), 8.01 (d, *J* = 8.4 Hz, 4H), 7.24 (d, *J* = 8.4 Hz, 4H), 5.65 (s, 2H), 4.83 (s, 2H), 4.26 (s, 5H), 4.00 ppm (s, 6H); elemental analysis: calcd (%) for $C_{47}H_{36}FeN_4O_3$: C 74.21, H 4.77, N 7.37; found: C 74.58, H 4.02, N 7.99.

14: FAB-MS: *m*/*z* (%): 697 (80%) $[M^+]$; ^{1}H NMR (400 MHz, $CDCl_3$, 25 °C, TMS): δ = 9.65 (d, *J* = 4.0 Hz, 1H), 9.40 (d, *J* = 4.0 Hz, 1H), 8.90–9.00 (m, 3H), 8.65 (d, *J* = 5.1 Hz, 1H), 8.45 (d, *J* = 4.0 Hz, 1H), 8.30 (d, *J* = 4.4 Hz, 1H), 8.20 (d, *J* = 8.0 Hz, 2H), 8.0 (d, *J* = 8.0 Hz, 2H), 7.34 (m, 4H), 5.75 (s, 2H), 4.82 (s, 2H), 4.3 (s, 5H), 4.10 (s, 6H), −1.42 ppm (br s, NH); elemental analysis: calcd (%) for $C_{43}H_{33}FeN_3O_3$: C 74.03, H 4.78, N 6.02; found: C 74.18, H 5.04, N 6.32.

The above procedure was followed by using the respective oxatripyrranes **5**–**8** with **3** to obtain other ferrocene–oxacorrole and ferrocene–oxasmaragdyrin conjugates.

10: FAB-MS: *m*/*z* (%): 729 (100%) $[M^+]$; ^{1}H NMR (400 MHz, $CDCl_3$, 25 °C, TMS): δ = 9.66 (d, *J* = 4.0 Hz, 2H), 9.27 (d, *J* = 4.0 Hz, 2H), 9.21 (d, *J* = 4.0 Hz, 2H), 8.56 (s, 2H), 8.25 (d, *J* = 4.0 Hz, 2H), 7.97 (d, *J* = 8.4 Hz, 4H), 7.52 (d, *J* = 8.4 Hz, 4H), 5.68 (s, 2H), 4.83 (s, 2H), 4.27 (s, 5H), 2.64 ppm (s, 6H); elemental analysis: calcd (%) for $C_{47}H_{36}FeN_4O$: C 77.47, H 4.98, N 7.69; found: C 77.03, H 5.10, N 7.49.

11: FAB-MS: *m*/*z* (%): 785 (100%) $[M^+]$; ^{1}H NMR (400 MHz, $CDCl_3$, 25 °C, TMS): δ = 9.66 (d, *J* = 4.0 Hz, 2H), 9.29 (d, *J* = 4.0 Hz, 2H), 9.22 (d, *J* = 4.0 Hz, 2H), 8.58 (s, 2H), 8.28 (d, *J* = 4.0 Hz, 2H), 8.01 (d, *J* = 8.4 Hz, 4H), 7.56 (d, *J* = 8.4 Hz, 4H), 5.68 (s, 2H), 4.82 (s, 2H), 4.27 (s, 5H), 3.20 (m, 2H), 1.49 (m, 6H), 1.47 ppm (m, 6H); elemental analysis: calcd (%) for $C_{51}H_{44}FeN_4O$: C 78.05, H 5.65, N 7.14; found: C 79.20, H 5.99, N 6.25.

12: FAB-MS: *m*/*z* (%): 813 (100%) $[M^+]$; ^{1}H NMR (400 MHz, $CDCl_3$, 25 °C, TMS): δ = 9.72 (d, *J* = 3.6 Hz, 2H), 9.45 (d, *J* = 3.6 Hz, 2H), 9.34 (d, *J* = 3.6 Hz, 2H), 8.64 (s, 2H), 8.33 (d, *J* = 3.6 Hz, 2H), 8.10 (d, *J* = 7.6 Hz, 4H), 7.77 (d, *J* = 7.6 Hz, 4H), 5.74 (s, 2H), 4.88 (s, 2H), 4.33 (s, 5H), 1.61 ppm (s, 18H); elemental analysis: calcd (%) for $C_{53}H_{48}FeN_4O$: C 78.32, H 5.95, N 6.89; found: C 76.58, H 4.92, N 7.09.

13: FAB-MS: *m*/*z* (%): 785 (100%) $[M^+]$; ^{1}H NMR (400 MHz, $CDCl_3$, 25 °C, TMS): δ = 9.63 (d, *J* = 4.4 Hz, 2H), 9.25 (d, *J* = 4.0 Hz, 2H), 9.18 (d, *J* = 4.4 Hz, 2H), 8.36 (s, 2H), 8.15 (d, *J* = 4.0 Hz, 2H), 7.16 (s, 4H), 5.66 (s, 2H), 4.79 (s, 2H), 4.24 (s, 5H), 2.55 (s, 6H), 1.85 (s, 12H), −2.43 ppm (br s, NH); elemental analysis: calcd (%) for $C_{51}H_{44}FeN_4O$: C 78.05, H 5.65, N 7.14; found: C 78.08, H 5.94, N 7.99.

15: FAB-MS: *m*/*z* (%): 664 (90%) $[M^+]$; ^{1}H NMR (400 MHz, $CDCl_3$, 25 °C, TMS): δ = 9.56 (d, *J* = 4.6 Hz, 1H), 9.33 (d, *J* = 4.4 Hz, 1H), 8.89 (d, *J* = 5.1 Hz, 1H), 8.86 (m, 2H), 8.58 (d, *J* = 5.1 Hz, 1H), 8.38 (d, *J* = 4.1 Hz, 1H), 8.22 (d, *J* = 4.6 Hz, 1H), 8.05 (d, *J* = 8.0 Hz, 2H), 7.90 (d, *J* = 8.0 Hz, 2H), 7.50 (d, *J* = 8.0 Hz, 2H), 7.46 (d, *J* = 8.0 Hz, 2H), 5.55 (s, 2H), 4.74 (s, 2H), 4.22 (s, 5H), 2.61 (s, 3H), 2.58 (s, 3H), −1.50 ppm (br s, NH); elemental analysis: calcd (%) for $C_{43}H_{33}FeN_3O$: C 77.59, H 4.78, N 6.31; found: C 77.28, H 4.62, N 6.44.

16: FAB-MS: *m*/*z* (%): 720 (100%) $[M^+]$; ^{1}H NMR (400 MHz, $CDCl_3$, 25 °C, TMS): δ = 9.56 (d, *J* = 4.4 Hz, 1H), 9.33 (d, *J* = 4.0 Hz, 1H), 8.93 (d, *J* = 5.2 Hz, 1H), 8.86 (m, 2H), 8.61 (d, *J* = 5.2 Hz, 1H), 8.41 (d, *J* = 4.2 Hz, 1H), 8.22 (d, *J* = 4.4 Hz, 1H), 8.11 (d, *J* = 8.0 Hz, 2H), 7.95 (d, *J* = 8.0 Hz, 2H), 7.56 (d, *J* = 8.0 Hz, 2H), 7.52 (d, *J* = 8.0 Hz, 2H), 5.56 (s, 2H), 4.75 (s, 2H), 4.23 (s, 5H), 4.15 (s, 2H), 1.48 (s, 3H), 1.46 (s, 3H), 1.45 (s, 3H), 1.43 (s, 3H) −1.50 ppm (br s, NH); elemental analysis: calcd (%) for $C_{47}H_{41}FeN_3O$: C 78.22, H 6.01, N 5.82; found: C 78.29, H 5.92, N 5.64.

17: FAB-MS: *m*/*z* (%): 748 (100%) $[M^+]$; ^{1}H NMR (400 MHz, $CDCl_3$, 25 °C, TMS): δ = 9.58 (d, *J* = 4.8 Hz, 1H), 9.33 (d, *J* = 4.8 Hz, 1H), 8.94 (d, *J* = 5.2 Hz, 1H), 8.86 (m, 2H), 8.61 (d, *J* = 5.2 Hz, 1H), 8.43 (d, *J* = 4.2 Hz, 1H), 8.23 (d, *J* = 4.8 Hz, 1H), 8.12 (d, *J* = 8.4 Hz, 2H), 7.96

(d, J = 8.4 Hz, 2H), 7.72 (d, J = 8.4 Hz, 2H), 7.68 (d, J = 8.4 Hz, 2H), 5.56 (s, 2H), 4.75 (s, 2H), 4.33 (s, 5H), 1.18 (s, 18H), −1.50 ppm (br s, NH); elemental analysis: calcd (%) for $C_{49}H_{45}FeN_3O$: C 78.49, H 6.32, N 5.60; found: C 78.28, H 6.42, N 5.81.

18: FAB-MS: m/z (%): 720 (60%) [M^+]; ^{1}H NMR (400 MHz, $CDCl_3$, 25°C, TMS): δ = 9.50 (d, J = 4.4 Hz, 1H), 9.37 (d, J = 4.4 Hz, 1H), 8.85 (d, J = 4.4 Hz, 1H), 8.81 (m, 2H), 8.46 (d, J = 4.4 Hz, 1H), 8.35 (d, J = 5.2 Hz, 1H), 8.15 (d, J = 4.4 Hz, 1H), 7.47(s, 1H), 7.45 (s, 1H), 7.28 (s, 2H), 5.56 (s, 2H), 4.74 (s, 2H), 4.20 (s, 5H), 2.52 (s, 3H), 2.51 (s, 3H), 1.82 (s, 6H), 1.77 (s, 6H), −1.50 ppm (br s, NH); elemental analysis: calcd (%) for $C_{47}H_{41}FeN_3O$: C 77.94, H 6.01, N 5.35; found: C 78.08, H 6.42, N 5.30.

[5,10-(*p*-Methoxydiphenyl)-19-ferrocenyl-25-oxasmaragdyrinato]dicarbonylrhodium(I) (19): Oxasmaragdyrin **9** (0.030 g, 0.04 mmol) was dissolved in alcohol-free dichloromethane (50 mL). Anhydrous sodium acetate (0.053 g, 0.40 mmol) was added to the solution, followed by di-μ-chlorobis[dicarbonylrhodium(I)] (0.023 g, 0.06 mmol), and the mixture was stirred under reflux for 2 h. The solvent was evaporated, then chromatographed on a silica gel column with dichloromethane solution. Removal of the solvent gave a purple solid (0.035 g, 98%), which was recrystallized from a dichloromethane/*n*-heptane mixture.

19: FAB-MS: m/z (%): 918 (70%) [M^+]; ^{1}H NMR (400 MHz, $CDCl_3$, 25°C, TMS): δ = 9.35 (m, 4H), 8.96 (d, J = 4.4 Hz, 2H), 8.67 (s, 2H), 8.37 (d, J = 4.4 Hz, 2H), 8.11 (d, J = 8.28 Hz, 4H), 7.97 (d, J = 8.28 Hz, 4H), 5.58 (s, 2H), 4.80 (s, 2H), 4.52 (s, 5H), 4.05 (s, 6H), −1.43 ppm (s, NH); UV/Vis (CH_2Cl_2): λ_{max} ($\varepsilon \times 10^{-4}$) ($mol^{-1}dm^3cm^{-1}$) = 461 (15.6), 491 (0.5), 589 (1.4), 629 (1.3), 653 (1.3), 719 nm (2.6) (2.14×10^{-6} M); IR (KBr): $\tilde{\nu}$ = 2007, 2072 cm^{-1} (C≡O).

5,10-(*p*-Methoxydiphenyl)-19-ferrocenyl-25-oxa-smaragdyrin, hydrochloride salt (20): Oxasmaragdyrin **9** (0.030 g, 0.039 mmol) was dissolved in dichloromethane (20 mL). The solution was worked up in a separating funnel with 10% HCl solution (20 mL). The organic layer was separated quickly, and dried over $MgSO_4$. Evaporation of solvent yielded a brown-green solid (0.027 g, 90%). This was further recrystallized from dichloromethane and *n*-heptane.

20: FAB-MS: m/z (%): 761 (100%) [M^+]; ^{1}H NMR (400 MHz, $CDCl_3$, 25°C, TMS): δ = 9.73 (d, J = 4.4 Hz, 2H), 9.38 (d, J = 3.6 Hz, 2H), 9.33 (d, J = 4.4 Hz, 2H), 9.00 (s, 2H), 8.40 (d, J = 3.6 Hz, 2H), 8.25 (d, J = 8.4 Hz, 4H), 8.13 (d, J = 8.4 Hz, 4H), 5.89 (s, 2H), 5.00 (s, 2H), 4.35 (s, 5H), 4.07 (s, 6H), −1.43 (br s, NH), −1.33 (br s, NH), −0.32 (br s, NH), −0.15 ppm (br s, NH); UV/Vis (CH_2Cl_2): λ_{max} ($\varepsilon \times 10^{-4}$) ($mol^{-1}dm^3cm^{-1}$) = 457 (7.3), 624 (0.4), 659 (0.8), 765 nm (2.3) (2.15×10^{-6} M).

Acknowledgement

This work was supported by grants from the Department of Science and Technology (DST) and the Council of Scientific and Industrial Research (CSIR), Government of India, New Delhi. We thank Dr. B. S. Joshi, CBMRI, SGPGI, Lucknow, for low-temperature ^{1}H NMR studies, and Dr. S. Nagendran for solving the crystal structure of **3**. R.K. and J.S. thank the CSIR for their fellowships.

[1] a) J. H. Chou, M. E. Kosal, H. S. Nalwa, N. A. Rakow, K. S. Suslick in *Porphyrin Handbook, Vol. VI*, (Eds.: K. M. Kadish, K. M. Smith, R. Guilard), Academic Press, San Diego, **1999**, Chapter 41, pp. 43–131; b) A. Tsuda, A. Osuka, *Science* **2001**, *293*, 79–82.

[2] a) L. M. Tolbert, X. Zhao, Y. Ding, L. A. Bottomley, *J. Am. Chem. Soc.* **1995**, *117*, 12891–12892; b) R. M. Metzger, C. A. Panetta, *New J. Chem.* **1991**, *15*, 209–221.

[3] S. Ery-Forgues, B. Nelvaux-Nicot, *J. Photochem. Photobiol. A* **2000**, *132*, 137–139.

[4] a) A. K. Burrell, W. M. Campbell, D. L. Officer, S. M. Scott, K. C. Gordon, M. R. McDonald, *J. Chem. Soc. Dalton Trans.* **1999**, 3349–3354; b) E. S. Schmidt, T. S. Calderwood, T. C. Bruice, *Inorg. Chem.* **1986**, *25*, 3718–3720; c) P. D. Beer, M. G. B. Drew, D. Hesek, R. Jagessar, *J. Chem. Soc. Chem. Commun.* **1995**, 1187–1189.

[5] a) N. M. Loim, N. V. Abramova, V. I. Sokolv, *Mendeleev Commun.* **1996**, 46–47; b) N. M. Loim, N. V. Abramova, R. Z. Khaliullin, Y. S. Lukashov, E. V. Vorontsov, V. I. Sokolov, *Russ. Chem. Bull.* **1998**, *107(47)*, 1016–1017; c) P. D. W. Boyd, A. K. Burrell, W. M. Campbell, P. A. Cocks, K. C. Gordon, G. B. O. Jameson, D. L. Officer, Z. Zhao, *Chem. Commun.* **1999**, 637–638; d) S. W. Rhee, B. B. Park, Y. Do, J. Kim, *Polyhedron* **2000**, *19*, 1961–1966; e) S. W. Rhee, Y. H. Na, Y. Do, J. Kim, *Inorg. Chim. Acta* **2000**, *309*, 49–56; f) C. Bucher, C. H. Devillers, J.-C. Moutet, G. Royal, E. Saint-Aman, *Chem. Commun.* **2003**, 888–889.

[6] R. G. Wollmann, D. N. Hendrickson, *Inorg. Chem.* **1977**, *16*, 3079–3089.

[7] a) S. J. Narayanan, S. Venkatraman, S. R. Dey, B. Sridevi, V. G. Anand, T. K. Chandrashekar, *Synlett* **2000**, *12*, 1834–1835; b) S. Venkatraman, V. Prabhuraja, R. Misra, R. Kumar, T. K. Chandrashekar, W. Teng, K. R. Senge, *Ind. J. Chem.* **2003**, *42*, 2191–2197.

[8] a) S. J. Narayanan, B. Sridevi, T. K. Chandrashekar, *Org. Lett.* **1999**, *1*, 587–590; b) B. Sridevi, S. J. Narayanan, T. K. Chandrashekar, U. Englich, K. R. Senge, *Chem. Eur. J.* **2000**, *6*, 2554–2563.

[9] T. D. Lash, S. T. Chancy, D. T. Richter, *J. Org. Chem.* **1998**, *63*, 9076–9088.

[10] a) S. J. Narayanan, B. Sridevi, T. K. Chandrashekar, U. Englich, K. R. Senge, *Inorg. Chem.* **2001**, *40*, 1637–1645; b) B. Sridevi, S. J. Narayanan, R. Rao, T. K. Chandrashekar, U. Englich, K. R. Senge, *Inorg. Chem.* **2000**, *39*, 3669–3677.

[11] J. Sankar, V. G. Anand, S. Venkatraman, H. Rath, T. K. Chandrashekar, *Org. Lett.* **2002**, *4*, 4233–4235.

[12] T. K. Chandrashekar, S. Venkatraman, *Acc. Chem. Res.* **2003**, *36*, 676–691.

[13] M. Ravikanth, D. Reddy, A. Mishra, T. K. Chandrashekar, *J. Chem. Soc. Dalton Trans.* **1993**, 1137–1141.

[14] M. Sheik-Bahae, A. A. Said, T. Hei, D. J. Hagan, W. Stryland, *IEEE J. Quantum Electron.* **1990**, *26*, 760–769.

[15] H. Hope, Prog. *Inorg. Chem.* **1994**, *41*, 1–19.

[16] a) G. M. Sheldrick, SHELXS-93f, Universität Gottingen, **1993**; b) G. M. Sheldrick, SHELXL-97, Universität Gottingen, **1997**.

[17] B. Sridevi, S. J. Narayanan, A. Srinivasan, M. V. Reddy, T. K. Chandrashekar, *J. Porphyrins Phthalocyanines* **1998**, *2*, 9076–9088.

Received: September 20, 2003
Revised: November 11, 2003 [F5558]